Significant results as of 2022-04

- Plasmonic interferometry is a rapidly growing area of research with a huge potential for applications in the terahertz frequency range. We designed a plasmonic interferometer based on graphene field effect transistor with its source and drain connected to sleeves of a bent bow-tie antenna. We observed helicity- and phase- sensitive conversion of circularly polarized radiation into dc photovoltage caused by the interference of two plasma waves inside the graphene channel, which were excited at the source and drain of the transistor. The helicity-sensitive phase shift between these waves was achieved by using an asymmetric antenna configuration. The dc signal changed sign with inversion of the helicity. The suggested plasmonic interferometer can measure the phase difference between two arbitrary phase-shifted optical signals. The observed effect allows for the phase-sensitive probing of the plasma wave excitations in two-dimensional materials. (Matyushkin, Y. *et al.* Helicity-Sensitive Plasmonic Terahertz Interferometer. *Nano Lett.* **20**, 7296–7303 (2020)).
-

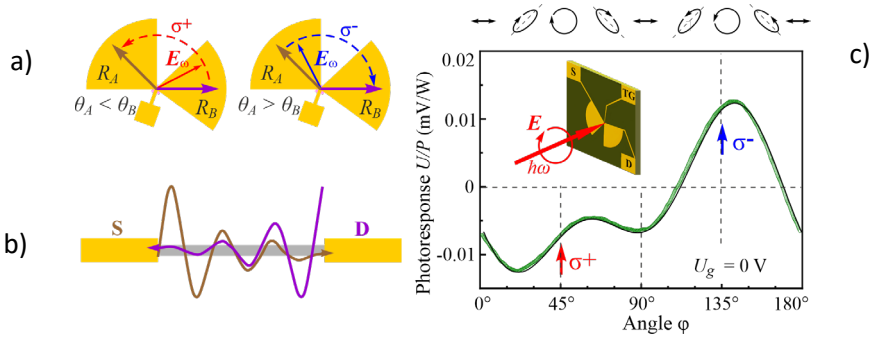

*Figure 1. (a, b) Illustration of the physics behind the circular photoresponse caused by the plasmonic interference: (a) Bent bowtie antenna characterized with two vectors RA and RB along with the hodograph of the electric field in the case of circular polarization for positive (left, red arrow) and negative (right, blue arrow) helicities. Due to the opposite rotation direction, the phase differences between the source and drain potentials have opposite signs for opposite helicities. (b) Illustration of plasma waves excited at the source and drain electrodes. (c) Helicity dependence of the photovoltage U(ϕ) normalized by the radiation power P. The inset shows the antenna layout relative to the incoming radiation with circular polarization. The photo-response changes sign when the helicity changes. Reprinted (adapted) with permission from (Y. Matyushkin, S. Danilov, M. Moskotin, V. Belosevich, N. Kaurova, M. Rybin, E. D. Obraztsova, G. Fedorov, I. Gorbenko, V. Kachorovskii, and S. Ganichev, Nano Lett. **20**, 7296 (2020)). Copyright 2020 American Chemical Society.)*

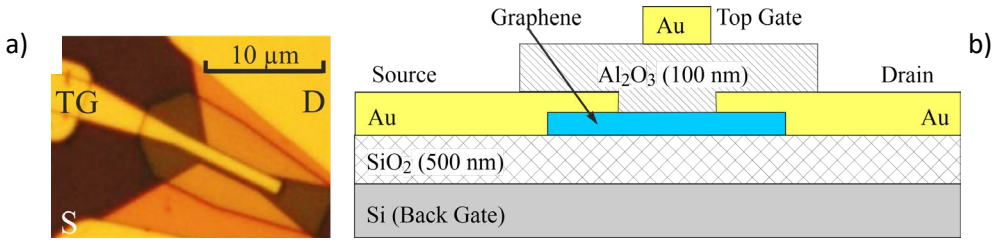

*Figure 2. Device configuration and characterization. (a) zoomed image of the device; (b) Structure cross-section showing relative location of the source, drain, and top gate electrodes as well as thickness of the dielectric layers. Reprinted (adapted) with permission from (Y. Matyushkin, S. Danilov, M. Moskotin, V. Belosevich, N. Kaurova, M. Rybin, E. D. Obraztsova, G. Fedorov, I. Gorbenko, V. Kachorovskii, and S. Ganichev, Nano Lett. **20**, 7296 (2020)). Copyright 2020 American Chemical Society.*

- As a next step, we demonstrated that the plasmonic interferometer can also be realized in carbon nanotube structures. This study also revealed that the presence of the helicity- and phase-sensitive interference part of the photovoltaic response is a universal phenomenon, which is obtained in the systems of different dimensionality with different single-particle spectrum. Its magnitude is a characteristic of the plasma wave decay length. We observed oscillations of the circular photoresponse as a function of the gate voltage. We developed a theory, which explains basic experimental results. Importantly, our theoretical analysis showed that this effect is universal in a sense that the helicity- and phase-sensitive part of the response is the same (up to unimportant numerical coefficients) in the systems of different dimensionalities with different single particle spectrum. For non-resonant regime, discussed in the current work, the magnitude of the response is fully controlled by the plasma wave decay length. This opens up a wide avenue for applications in the area of plasmonic interferometry. (Matyushkin, Y. *et al.* Carbon nanotubes for polarization sensitive terahertz plasmonic interferometry, *Opt. Express* ***29****(23), 37189 (2021)).*

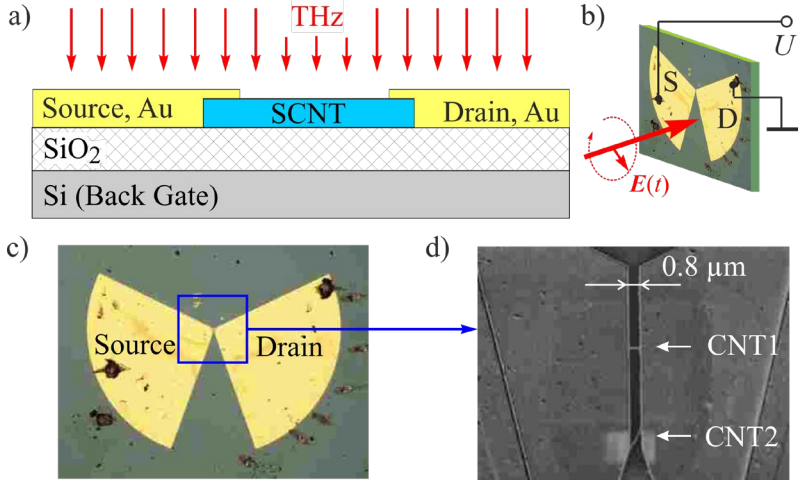

Figure 3. Devices configuration and characterization. (a) Structures cross-section. (b) Experimental set-up. (c) and (d) Optical and scanning electron microscopy (SEM) images illustrating the device layout with source and drain electrodes connected to sleeves of a bent bow-tie antenna. The two individual CNT seen in the (d) have the lengths of 0.8 μm (upper one) and 2.8 μm (lower one). There diameters lie in the range from 2 to 4 nm. Reprinted (adapted) with permission from (Y. Matyushkin, S. Danilov, M. Moskotin, G. Fedorov, A. Bochin, I. Gorbenko, V. Kachorovskii, and S.Ganichev, Carbon nanotubes for polarization sensitive terahertz plasmonic interferometry, Opt. Express ***29****(23), 37189 (2021)*

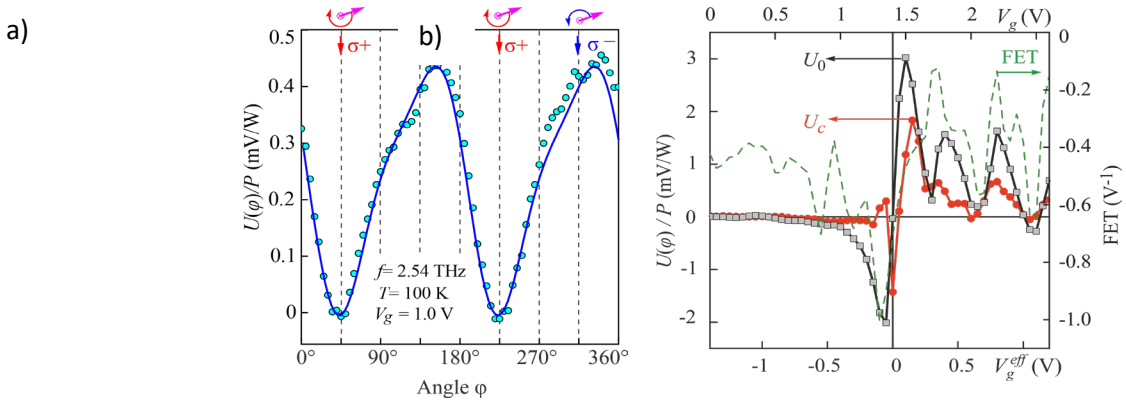

Figure 4. (a) Helicity dependence of the photovoltage U(φ) normalized by the laser radiation power P. Downward arrows labelled σ⁺ and σ⁻ indicate angles φ corresponding to the clockwise and anticlockwise rotating in-plane electric field E(t) of the right- and left-handed circularly polarized radiation, respectively. The arrows on top illustrate the rotation of the electric field vector for σ⁺ (φ = 45 and 225 degrees) and σ⁻ (φ = 135 and 315 degrees). (b) Gate voltage dependencies of

*the circular (U_c) and polarization insensitive (U_0) photo response normalized on the laser power P. Considered that for the circularly polarized radiation the helicity sensitive contribution changes its sign, whereas U_0 remains unchanged and $U_{L1} = U_{L2} = 0$ (both degrees of linear polarization are zero), we calculated the amplitude after $U_c = (U_{\sigma+} - U_{\sigma-})/2$ and $U_0 = (U_{\sigma+} + U_{\sigma-})/2$. Upper scale indicates the gate voltages V_g and bottom scale indicates the corresponding effective gate voltages V^{eff}. Vertical line indicates the position of the CNP ($V^{eff} = 0$). Reprinted (adapted) with permission from (Y. Matyushkin, S. Danilov, M. Moskotin, G. Fedorov, A. Bochin, I. Gorbenko, V. Kachorovskii, and S.Ganichev, Carbon nanotubes for polarization sensitive terahertz plasmonic interferometry, Opt. Express **29**(23), 37189 (2021)*

- In Hall bar graphene structures, we observed and study of the circular transverse photoconductivity in graphene induced by terahertz radiation of moderate and large intensity. We demonstrate that absorption of the terahertz radiation results in a Hall photocurrent whose direction changes to the opposite with inversion of either the bias voltage polarity or the radiation helicity. The detected Hall photoresponse is negligibly small at the charge neutrality point (CNP). At low gate voltages away from the CNP, the photoresponse is proportional to the radiation intensity I at low intensities sometimes saturating at higher I. Such behavior is consistent with theory predicting the circular transverse photoconductivity of second order in the radiation electric field E. Strikingly, at high electron densities corresponding to higher gate voltages, the observed Hall photosignals exhibit a superlinear intensity dependence and vary as I^2. Such behavior is detected for several frequencies ranging from 0.78 to 3.33 THz. Unlike the transverse photoconductivity, the longitudinal photoconductivity signal measured parallel to the bias current was insensitive to the radiation helicity. We discuss the observed THz radiation-induced circular Hall effect in terms of intraband electron kinetics in the presence of static and circular high-frequency electric fields. The corresponding quasiclassical theory is consistent with our experimental results at low gate voltages and clarifies why the linear-in-I contributions show up away from the CNP and can drop down at high gate voltages. An extension of this theory to higher orders is required to explain the emergence of strong quadratic-in-I contributions to the circular Hall effect dominating the observed THz photosignals at high gate voltages and high intensities. (*S. Candussio et al., THz radiation induced circular Hall effect in graphene, Phys. Rev. B (2022), arXiv:submit/4146638*)

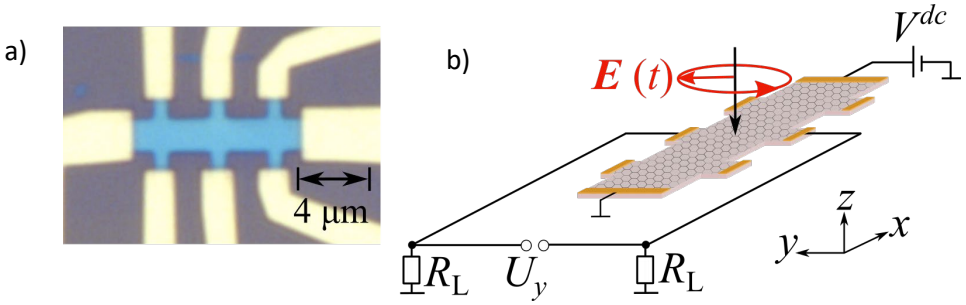

Figure 5. (a) A microscope image of the Hall bar structure. (b) The experimental setup. The sample is irradiated with circularly polarized light along z-direction at normal to the sample surface. A dc bias voltage V^{dc} is applied in x direction along the Hall bar. The transversal photosignal U_y is picked up as a voltage drop over load resistors $R_L = 50\ \Omega$. Reprinted (adapted) with permission from (S. Candussio, S. Bernreuter, T. Rockinger, K. Watanabe, T.Taniguchi, J. Eroms, I.A. Dmitriev, D. Weiss, and S.D. Ganichev, THz radiation induced circular Hall effect in graphene, Phys. Rev. B (2022), arXiv:2202.0113v1 [cond-mat.mes-hall])

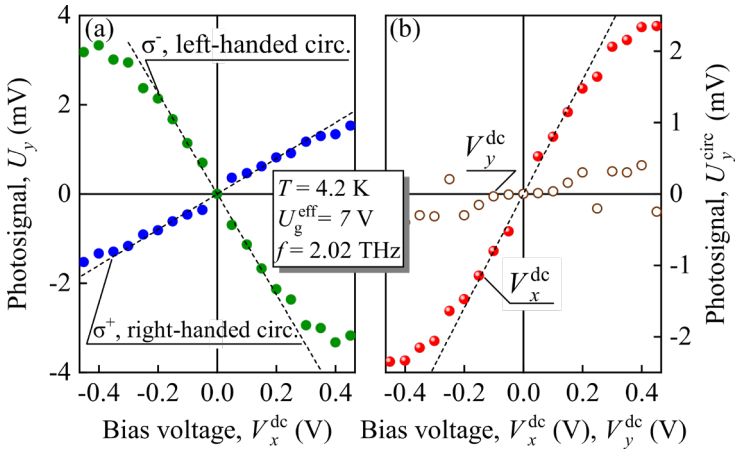

Figure 6. (a) Transversal photosignal picked up perpendicular to the direction of the applied dc bias voltage V^{dc} which is swept at a fixed gate voltage of 7 V for right- and left-handed circularly polarized light. (b) The calculated helicity dependent parts of the Hall signal (dc bias voltage V^{dc} along x, full dots) and of the longitudinal signal (dc bias voltage V^{dc} along y, open dots). Dashed linear fits are a guide for the eye. Reprinted (adapted) with permission from (S. Candussio, S. Bernreuter, T. Rockinger, K. Watanabe, T.Taniguchi, J. Eroms, I.A. Dmitriev, D. Weiss, and S.D. Ganichev, THz radiation induced circular Hall effect in graphene, Phys. Rev. B (2022), arXiv:2202.0113v1 [cond-mat.mes-hall])

- We observed the magnetic quantum *ratchet effect* in graphene with a lateral dual-grating top gate (DGG) superlattice. The THz ratchet current demonstrated sign-alternating magneto-oscillations due to the Shubnikov–de Haas effect. The amplitude of these oscillations was greatly enhanced as compared to the ratchet effect at zero magnetic field. The direction of the current was determined by the lateral asymmetry which could be controlled by variation of gate potentials in DGG. The dependence of the ratchet current on the orientation of the terahertz electric field (for linear polarization) and on the radiation helicity (for circular polarization) was also studied. Notably, in the latter case, switching from the right- to left-circularly polarized radiation resulted in the inversion of the photocurrent direction. These observations could be modelled using the drift-diffusion approximation in the Boltzmann kinetic equation and taking into account the Landau quantization. (Hubmann, S. *et al.* Giant ratchet magneto-photocurrent in graphene lateral superlattices. *Phys. Rev. Res.* **2**, 033186 (2020)).

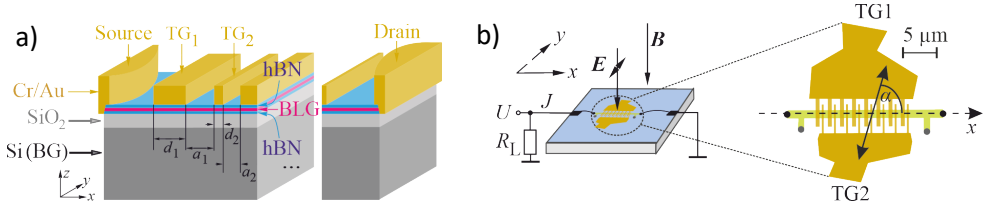

*Figure 8. (a) Sketch of the sample structure and the dual-grating gate superlattice. (b) Sketch of the experimental setup for the ratchet photocurrent measurements and sketch of the superlattice (top view). Black dots show electric contacts to graphene layer. Reprinted (adapted) with permission from (S. Hubmann, V. V. Bel'kov, L. E. Golub, V. Y. Kachorovskii, M. Drienovsky, J. Eroms, D. Weiss, and S. D. Ganichev, Giant ratchet magneto-photocurrent in graphene lateral superlattices, Phys. Rev. Res. **2**, 033186 (2020))*

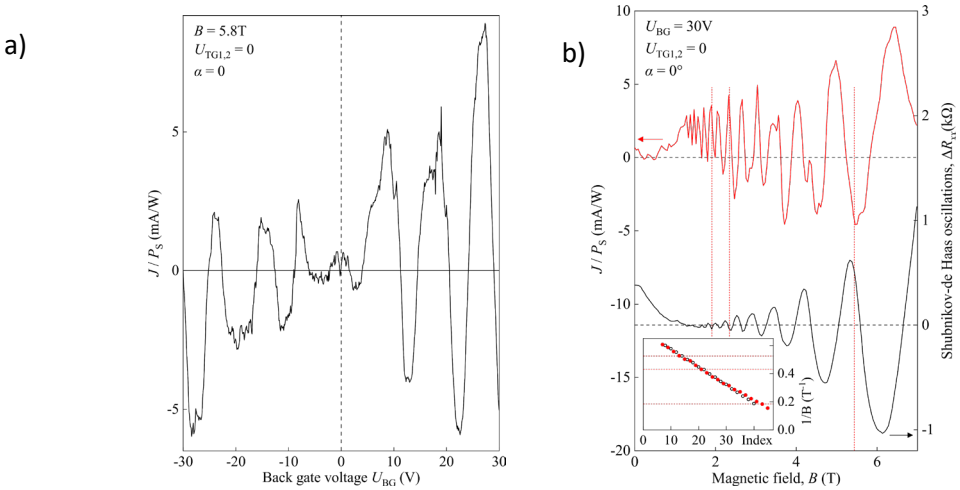

*Figure 9. (a) Dependence of the ratchet photocurrent normalized to the radiation power coming onto the sample on the voltage applied to the back gate. The data are obtained for linear polarization with α = 0. (b) The photocurrent normalized to the radiation power coming onto the sample and the SdH longitudinal resistance oscillations as functions of magnetic field B. The oscillatory part was obtained by subtracting a polynomial background of the form $A_0 + C B^2 + D B^4$ from the longitudinal resistance R_{xx} (B). The coefficients A_0, C, and D were obtained by fitting to the high field data. Vertical dashed lines mark some of the oscillations' extrema positions. The inset shows corresponding positions of transport (black circles) and photocurrent oscillations (red dots) on a 1/B scale as a function of the extremum's index. Horizontal dashed lines correspond to the vertical lines in the main plot. Reprinted (adapted) with permission from (S. Hubmann, V. V. Bel'kov, L. E. Golub, V. Y. Kachorovskii, M. Drienovsky, J. Eroms, D. Weiss, and S. D. Ganichev, Giant ratchet magneto-photocurrent in graphene lateral superlattices, Phys. Rev. Res. **2**, 033186 (2020))*

- Graphene is a quantum spin Hall insulator with a 45 µeV wide non-trivial topological gap induced by the intrinsic spin-orbit coupling. Even though this zero-field splitting is weak, it makes graphene an attractive candidate for applications in quantum technologies, given the resulting long spin relaxation time. On the other side, the staggered sub-lattice potential, due for instance to the coupling of graphene with its boron nitride substrate, competes with the intrinsic spin-orbit potential and may lead to a trivial band insulator state. The full characterization of these potentials is therefore of great importance for understanding the details of the topological properties of graphene. Using a photoconductivity based electron spin resonance technique in the sub-Terahertz frequency domain, that we developped during DeMeGras project, we measure these two zero-field splittings in THz detectors based on graphene. Interestingly, we observe a significant increase of these potentials by lowering the temperature of the sample. We interpret this phenomenon by considering a thermal strain of the sample due to the difference between the thermal expansion coefficients of graphene and that of the metal grating on top of the graphene-based device. This strain not only breaks the sub-lattice potential by displacing the carbon atoms, but it also stretches the lattice and therefore affect the mixing of the different atomic orbitals, thus changing the intrinsic spin-orbit coupling.

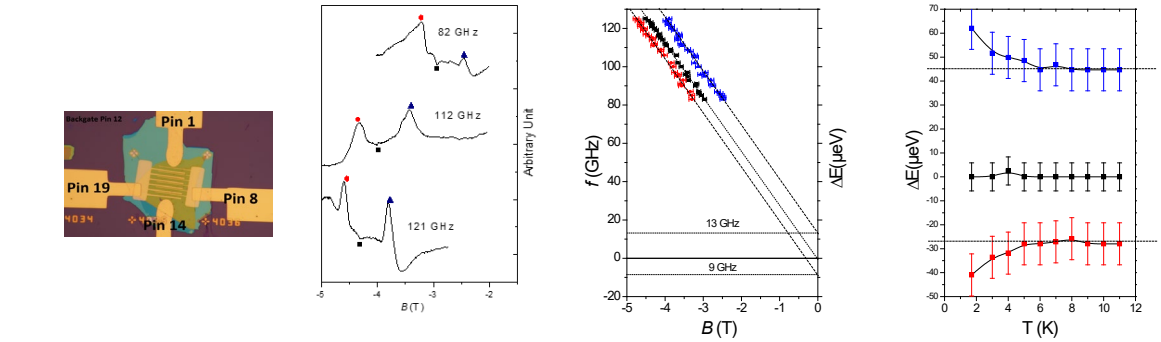

a) b) c) d)

Figure 10. (a) The ratchet graphene structure, which was used in the experiments. (b) The spin resonances in the photoconductivity at THz frequencies and magnetic field. (c) Extrapolation of the resonance frequencies to the zero magnetic field reveals the zero-split energy gap in graphene. (d) Unexpected temperature dependence of the resonances reveals a possible strain in graphene. Reprinted (adapted) with permission from (Temperature Tunable Zero-Field Splittings in Graphene-based THz detectors, C. Bray, C. Consejo, K. Maussang, J. A. Delgado Notario, I. Yahniuk, S. Krishtopenko, S. Ruffenach, S. Gebert, J. Torres, E. Moench, K. Indykiewicz, A. Yurgens, S. Ganichev, F. Teppe – in preparation (2022)

- In the simple graphene radiation detector (Fig. 11a), there are usually two identical *p-n* junctions created in the vicinity of the electrodes/antennas due to a proximity to the metal. It has been found that a small dc current induced additional heating in one- and cooling in another *p-n* junction (Fig. 11b) thereby breaking the initial symmetry of the structure. Due to the induced asymmetry, the ac current gets rectified giving a significantly increased signal (Fig. 11c). This allows to control the overall sensitivity of the detector to the external THz radiation.

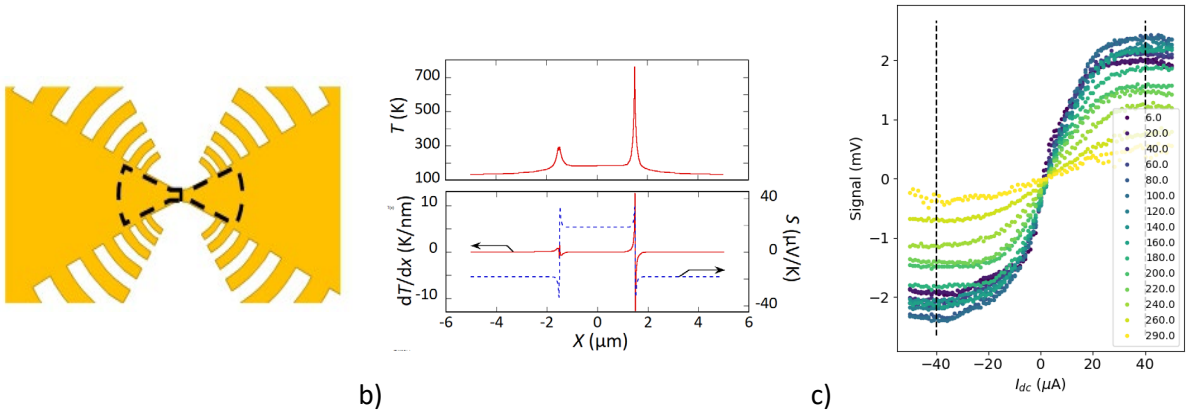

a) b) c)

Figure 11. (a) The symmetric graphene structure with two electrodes shaped into a log-periodic or bowtie antenna. (b) Calculated spatial distribution of the temperature (top) and temperature gradient and Seebeck coefficient (bottom) for some non-zero dc current flowing through the structure. (c) Rectification of the ac current induced by the radiation at 94 GHz. Reprinted (adapted) with permission from (K. Indykiewicz, …, F. Teppe, S.D. Ganichev, and A. Yurgens, in preparation (2022))

- The effectiveness of the thermoelectric readout mechanism in graphene radiation detectors was estimated for a few key parameters, assuming a simple device geometry, by solving the simple heat-diffusion equation:

$$-\frac{\partial}{\partial x}\left(\kappa_e \frac{\partial T}{\partial x}\right) = \frac{j^2}{\sigma} - jT\frac{\partial S}{\partial x} - \alpha_i\left(T^i - T_0^i\right)$$

The residual charge density and sharpness of the *p-n* junction are the main parameters that affect the detector performance most. In all cases, there is a trade-off between the responsivity and the total device resistance. These results showed that the thermoelectric readout in graphene radiation detectors represents a very competitive platform for building simple and sensitive direct detectors of radiation and arrays of them.

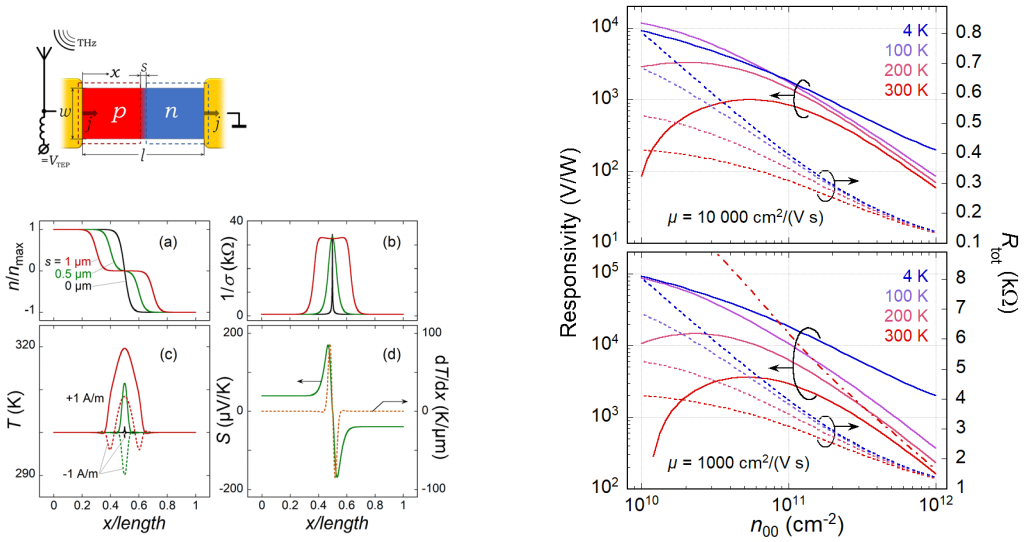

*Figure 13. Left top: the model geometry of graphene detector with a p-n junction in the center. Left bottom: (b) The doping profile. (c) The local sheet resistance. (c) The temperature distributions for j = +1 and −1 A/m (solid and dashed curves, respectively). The Peltier effect is a significant source of the temperature variations. (d) The temperature gradient (orange) and Seebeck coefficient calculated from (a,c). Right: The responsivity (left ordinate, solid lines) and overall detector resistance NEP (right ordinate, dotted lines) versus residual charge density due to charge puddles (n00) for different ambient temperatures and mobilities of 10000- (top) and 1000 cm²/V/s (bottom). Reprinted (adapted) with permission from (A. Yurgens, Sensors **20**(7), 1930 (2020))*

- Terahertz photoconductivity has been studied in magnetic fields in epitaxial graphene grown on 4H-SiC(1000) substrates. The dependence of the photoresponse signal on the magnetic field has been measured for different values of electron concentration, bias current, and terahertz radiation intensity. The photoconductivity mechanism based on the heating of electrons by terahertz radiation explains the experimental results. A strong increase in the photoconductivity signal at magnetic fields was detected due to suppression of electron-electron scattering. In this study, we presented the results of investigations of the terahertz photoconductivity in epitaxial graphene grown by thermal sublimation on the 4H-SiC(1000) surface. The investigations were carried out on meander-shaped structures with a length-to- width ratio of 600. The photoresponse in a magnetic field at different electron densities, bias currents, and terahertz-radiation intensities was examined. The occurrence of the photoconductivity was explained by the heating of carriers as a result of terahertz-radiation absorption. A strong increase in the photoconductivity signal due to weakening of the electron-electron scattering in a magnetic field was detected. (Vasiliev, Y. B., Novikov, S. N., Danilov, S. N. & Ganichev, S. D. Terahertz Photoconductivity in Graphene in a Magnetic Field. *Semiconductors* **54**, 465–470 (2020) and Baryshnikov, K. A., Vasilyev, Y. B., Novikov, S., Danilov, S. N. & Ganichev, S. D. Terahertz photoconductivity enhancement in graphene in magnetic fields. in *Journal of Physics: Conference Series* vol. 1482, 12039 (Institute of Physics Publishing, 2020))

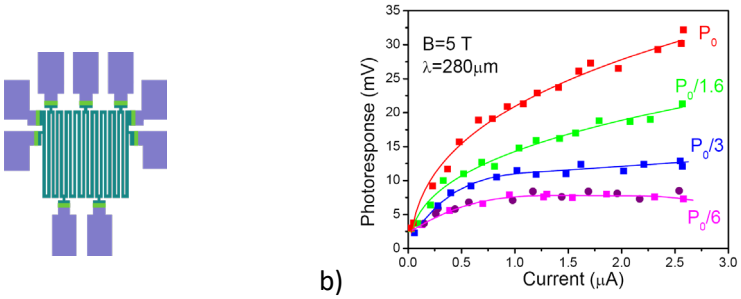

Figure 8. (a) Meander shape of the sample with a stripe width of 25 μm and a total length of 15 mm. (b) Bias current dependences of the photoconductivity-signal amplitude ΔV. The dependences for a radiation wavelength of 280 μm at different terahertz-radiation powers in a magnetic field of B = 5 T are shown. Circles and squares for the power $P_0/6$ correspond to measurements performed with different contacts. Reprinted (adapted) with permission from (Vasiliev, Y. B., Novikov, S. N., Danilov, S. N. & Ganichev, S. D. Terahertz Photoconductivity in Graphene in a Magnetic Field. Semiconductors 54, 465–470 (2020))

Publications

- S. Hubmann, V. V. Bel'kov, L. E. Golub, V. Y. Kachorovskii, M. Drienovsky, J. Eroms, D. Weiss, and S. D. Ganichev, *Giant ratchet magneto-photocurrent in graphene lateral superlattices,* Phys. Rev. Res. **2**, 033186 (2020); DOI: 10.1103/PhysRevResearch.2.033186.
- Y. Matyushkin, S. Danilov, M. Moskotin, V. Belosevich, N. Kaurova, M. Rybin, E. D. Obraztsova, G. Fedorov, I. Gorbenko, V. Kachorovskii, and S. Ganichev, *Helicity-Sensitive Plasmonic Terahertz Interferometer,* Nano Lett. 20, 7296 (2020); DOI: 10.1021/acs.nanolett.0c02692.
- Y. B. Vasiliev, S. N. Novikov, S. N. Danilov, and S. D. Ganichev, *Terahertz Photoconductivity in Graphene in a Magnetic Field,* Semiconductors 54, 465 (2020);DOI: 10.1134/S106378262004020X.
- K. A. Baryshnikov, Y. B. Vasilyev, S. Novikov, S. N. Danilov, and S. D. Ganichev, in J. Phys. Conf. Ser. (Institute of Physics Publishing, 2020), p. 12039;DOI: 10.1088/1742-6596/1482/1/012039.
- V. Galeeva, D. A. Belov, A. S. Kazakov, A. V. Ikonnikov, A. I. Artamkin, L. I. Ryabova, V. V. Volobuev, G. Springholz, S. N. Danilov, and D. R. Khokhlov, *Photoelectromagnetic Effect Induced by Terahertz Laser Radiation in Topological Crystalline Insulators Pb1-xSnxTe,* Nanomaterials 11, 3207 (2021), 11, 3207. DOI: https://doi.org/10.3390/nano11123207
- Y. Matyushkin, S. Danilov, M. Moskotin, G. Fedorov, A. Bochin, I. Gorbenko, V. Kachorovskii, and S. Ganichev, *Carbon nanotubes for polarization sensitive terahertz plasmonic interferometry,* Opt. Express 29(23), 37189 (2021); DOI: https://doi.org/10.1364/OE.435416
- S. Candussio, S. Bernreuter, T. Rockinger, K. Watanabe, T.Taniguchi, J. Eroms, I.A. Dmitriev, D. Weiss, and S.D. Ganichev, *THz radiation induced circular Hall effect in graphene,* Phys. Rev. B (2022), arXiv:submit/4146638 [cond-mat.mes-hall]
- M. Otteneder, M. Hild, Z. D. Kvon, E. E. Rodyakina, M. M. Glazov, S. D. Ganichev, *Highly superlinear giant terahertz photoconductance in GaAs quantum point contacts in the deep tunneling regime,* Phys. Rev. B 104, 205304 (2021).DOI:https://doi.org/10.1103/PhysRevB.104.205304
- S.V. Morozov, V.V. Rumyantsev, M.S. Zholudev, A A. Dubinov, V. Ya. Aleshkin, V. V. Utochkin, M. A. Fadeev, K. E. Kudryavtsev, N. N. Mikhailov, S. A. Dvoretskii, V. I. Gavrilenko, and F Teppe. *Coherent Emission in the Vicinity of 10 THz due to Auger-Suppressed Recombination of Dirac Fermions in HgCdTe Quantum Wells* - ACS Photonics 8 (12), 3526-3535 (2021) - https://doi.org/10.1021/acsphotonics.1c01111

- S.S. Krishtopenko, A.M. Kadykov, S. Gebert, S. Ruffenach, C. Consejo, J. Torres, C. Avogadri, B. Jouault, W. Knap, N.N. Mikhailov, S.A. Dvoretskii, and F. Teppe *Many-particle effects in optical transitions from zero-mode Landau levels in HgTe quantum wells,* - Physical. Review. B 102 (4), 041404 (2020) - https://doi.org/10.1103/PhysRevB.102.041404
- S. Mantion, C. Avogadri, S.S. Krishtopenko, S. Gebert, S. Ruffenach, C. Consejo, S.V. Morozov, N.N. Mikhailov, S.A. Dvoretskii, W. Knap, S. Nanot, F. Teppe, B. Jouault, *Quantum Hall states in inverted HgTe quantum wells probed by transconductance fluctuations,* - Physical Review B 102 (7), 075302 (2020); - https://doi.org/10.1103/PhysRevB.102.075302
- A. Yurgens, *Large Responsivity of graphene radiation detectors with thermoelectric readout: Results of simulations.* Sensors, 20(7), 1930 (2020); https://doi.org/10.3390/s20071930.
- M. Khan, K. Indykiewicz, P. L. Tam, and A. Yurgens, *High Mobility Graphene on EVA/PET,* Nanomaterials 12, 331 (2022); https://doi.org/10.3390/nano12030331.

Data creation

www.epub.uni-regensburg.de; one needs to switch to English and in the search field write "FLAG-ERA" or "DeMeGRaS"

Outreach and other activities

- Travel grant of VW Stiftung supporting cooperation of German and Ukraine scientists
- Regensburg 2 PhD both with great praise (S. Hubmann, M. Otteneder) plus one PhD almost finished (S. Candussio), Seminars, No exchange and travelling due to the pandemic.
- Montpellier hired Ukrainian engineer to help the French research team and to develop his skills with novel and unique THz experimental setups in the frame of DeMeGras, and MUSE action of Montpellier University allows him to keep his job waiting for his next position.
- Web page of the project: https://www.chalmers.se/en/departments/mc2/research/demegras/Pages/default.as. The inconvenience with having a long name of the homepage is compensated by the free support offered by Chalmers IT service.
- Graphene radiation detectors were included in the course Graphene science and technology (MCC130) of the Master's program Nanotechnology (Chalmers University of Technology)

…